J|A|C|S
ARTICLES
Published on Web 07/13/2006

How an Enzyme Tames Reactive Intermediates: Positioning of the Active-Site Components of Lysine 2,3-Aminomutase during Enzymatic Turnover As Determined by ENDOR Spectroscopy

Nicholas S. Lees,[‡] Dawei Chen,[§] Charles J. Walsby,[†] Elham Behshad,[§] Perry A. Frey,*[,§] and Brian M. Hoffman*[,‡]

Contribution from the Department of Chemistry, Northwestern University, 2145 Sheridan Road, Evanston, Illinois 60208, Department of Biochemistry, University of Wisconsin—Madison, 1710 University Avenue, Madison, Wisconsin 53726, and Department of Chemistry, Simon Fraser University, 8888 University Drive, Burnaby, British Columbia, Canada V5A 1S6

Received March 2, 2006; E-mail: bmh@northwestern.edu

Abstract: Lysine 2,3-aminomutase (LAM) utilizes a [4Fe-4S] cluster, *S*-adenosyl-L-methionine (SAM), and pyridoxal 5′-phosphate (PLP) to isomerize L-α-lysine to L-*β*-lysine. LAM is a member of the radical-SAM enzyme superfamily in which a $[4Fe\text{-}4S]^{+}$ cluster reductively cleaves SAM to produce the 5′-deoxyadenosyl radical, which abstracts an H-atom from substrate to form 5′-deoxyadenosine (5′-Ado) and the α-Lys• radical (state **3** (Lys•)). This radical isomerizes to the *β*-Lys• radical (state **4**(Lys•)), which then abstracts an H-atom from 5′-Ado to form *β*-lysine and the 5′-deoxyadenosyl radical; the latter then regenerates SAM. We use ^{13}C, $^{1,2}H$, ^{31}P, and ^{14}N ENDOR to characterize the active site of LAM in intermediate states that contain the isomeric substrate radicals or analogues. With L-α-lysine as substrate, we monitor the state with *β*-Lys•. In parallel, we use two substrate analogues that generate stable analogues of the α-Lys• radical: *trans*-4,5-dehydro-L-lysine (DHLys) and 4-thia-L-lysine (SLys). This first glimpse of the motions of active-site components during catalytic turnover suggests a possible major movement of PLP during catalysis. However, the principal focus of this work is on the relative positions of the carbons involved in H-atom transfer. We conclude that the active site facilitates hydrogen atom transfer by enforcing van der Waals contact between radicals and their reacting partners. This constraint enables the enzyme to minimize and even eliminate side reactions of highly reactive species such as the 5′-deoxyadensosyl radical.

Introduction

Lysine 2,3-aminomutase (LAM) uses a [4Fe-4S] cluster, *S*-adenosyl-L-methionine (SAM), and pyridoxal 5′-phosphate (PLP) in catalyzing the isomerization of L-α-lysine into L-*β*-lysine (Scheme 1). LAM is a member of the radical-SAM enzyme superfamily in which a $[4Fe\text{-}4S]^{+}$ cluster reductively cleaves SAM to generate the highly reactive 5′-deoxyadenosyl radical species. A further role of the [4Fe-4S] cluster, anchoring SAM through coordination of its methionine end to a non-cysteinyl-coordinated cluster-Fe via a classical five-membered N,O chelate ring, was discovered by ENDOR spectroscopy (pyruvate formate-lyase activating enzyme (PFL-AE),[1,2] LAM[3]) and more recently visualized by X-ray structure determination (coproporphyrinogen III oxidase,[4] biotin synthase,[5] MoaA,[6] LAM[7]). Analysis of ^{13}C and ^{2}H ENDOR from the labeled sulfonium methyl of SAM coordinated to PFL-AE[1] and LAM[3] demonstrated that the sulfonium group is held close to the cluster. This led us to propose that electron transfer from the reduced cluster of LAM state **1** cleaves the C5′—S bond of SAM to form the 5′-deoxyadenosyl radical of state **2**, while the sulfur of methionine becomes the sixth ligand to the unique iron.[3]

Scheme 1

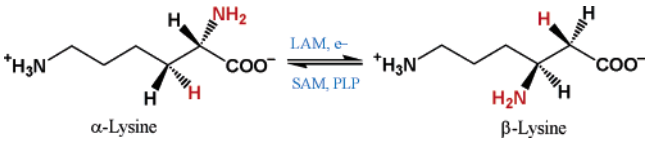

The arrangement of the cofactors and substrate of LAM in state **0** of its catalytic cycle (Scheme 2) prior to reduction of the $[4Fe\text{-}4S]^{2+}$ is shown in Figure 1.[7] The methods of choice for determining the corresponding information about steps **2**—**4**

[‡] Northwestern University.
[§] University of Wisconsin—Madison.
[†] Simon Fraser University.

(1) Walsby, C.; Hong, W.; Broderick, W. E.; Creek, J.; Ortillo, D.; Broderick, J. B.; Hoffman, B. *J. Am. Chem. Soc.* **2002**, *124*, 3143—3151.
(2) Walsby, C. J.; Ortillo, D.; Broderick, W. E.; Broderick, J. B.; Hoffman, B. M. *J. Am. Chem. Soc.* **2002**, *124*, 11270—11271.
(3) Chen, D.; Walsby, C.; Hoffman, B. M.; Frey, P. A. *J. Am. Chem. Soc.* **2003**, *125*, 11788—11789.
(4) Layer, G.; Moser, J.; Heinz, D. W.; Jahn, D.; Schubert, W.-D. *EMBO J.* **2003**, *22*, 6214—6224.
(5) Berkovitch, F.; Nicolet, Y.; Wan, J. T.; Jarrett, J. T.; Drennan, C. L. *Science (Washington, DC)* **2004**, *303*, 76—80.
(6) Haenzelmann, P.; Schindelin, H. *Proc. Natl. Acad. Sci. U.S.A.* **2004**, *101*, 12870—12875.
(7) Lepore, B. W.; Ruzicka, F. J.; Frey, P. A.; Ringe, D. *Proc. Natl. Acad. Sci. U.S.A.* **2005**, *102*, 13819—13824.

Scheme 2

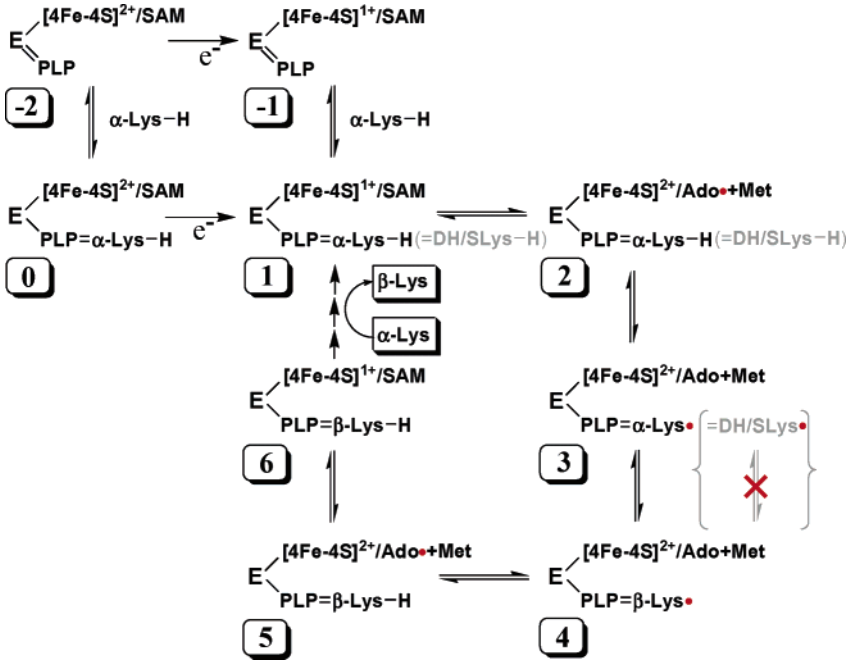

of the catalytic cycle are ENDOR/ESEEM spectroscopies.[8] When lysine and the other reaction components (PLP, SAM) are present, the reductive cleavage of SAM generates an equilibrium distribution of states which is accompanied by EPR signals from the paramagnetic species in their equilibrium concentrations. The dominant signal is from the [4Fe-4S]$^{+}$ cluster spin of state **1**. Because of the high reactivity of the 5′-deoxyadenosyl radical, state **2** does not accumulate when SAM itself is present. However, an analogue of SAM has been used to study the arrangement of the reactive components in state **2** by ESEEM.[9] Here we report the application of ENDOR spectroscopy to probe the relative geometries of the reactive components in the active site of LAM at even later stages in the enzymatic cycle: states **3** and **4**.

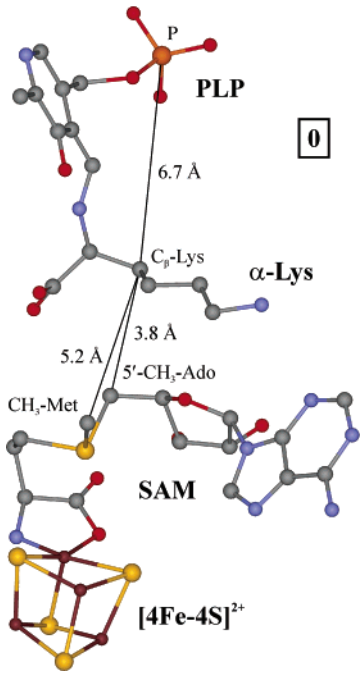

Figure 1. Arrangement of LAM cofactors in state **0**.[7]

Although state **2** does not accumulate during turnover of lysine by LAM, the steady-state EPR spectrum does include a small radical signal from the equilibrium concentration of the β-Lys$^{\bullet}$ radical (radical on the α-carbon),[10] and ENDOR measurements on this signal are used here to probe state **4**, denoted **4**(Lys$^{\bullet}$) (Scheme 2). To visualize state **3**, we have used two substrate analogues that generate stable analogues of the α-Lys$^{\bullet}$ radical: the inhibitors *trans*-4,5-dehydro-L-lysine (DHLys) and 4-thia-L-lysine (SLys).[11,12] H-atom abstraction from the β-carbon of each of these compounds during enzymatic reaction generates a stable radical with EPR signal at $g \approx 2.0$, a β-carbon 2pπ radical for SLys (SLys$^{\bullet}$), and an allylic radical delocalized over $\beta-\delta$-carbons in the case of DHLys (DHLys$^{\bullet}$) (Scheme 3).[11−13] As the spin-bearing p_z orbital on the SLys$^{\bullet}$ radical is located on the β-carbon,[13] as with α-Lys$^{\bullet}$, state **3**(SLys$^{\bullet}$) is a strict analogue of state **3**(Lys$^{\bullet}$); the **3**(DHLys$^{\bullet}$) allylic radical has approximately half the spin on the β-carbon and the other half on the δ-carbon.

With the substrate/analogue radicals as paramagnetic probes of states **3** and **4**, we report here the use of ^{13}C, ^{1,2}H, ^{31}P, and ^{14}N ENDOR to determine the positions of the components of SAM and of PLP relative to the radical site. Comparison of these results with the X-ray crystal structure of state **0** and ENDOR studies of states −**1** and **2** permits a first glimpse of the motions of active-site components during catalytic turnover, including a possible major movement of PLP during catalysis. The principal focus, however, is on the relative positions of the carbons involved in H-atom transfer. This study shows how enzyme−substrate binding interactions remote from a radical

(8) Schweiger, A.; Jeschke, G. *Principles of Pulse Electron Paramagnetic Resonance*; Oxford University Press: Oxford, UK, 2001.
(9) Magnusson, O. Th.; Lees, N. S.; Frey, P. A.; Reed, G. H.; LoBrutto, R., manuscript in preparation
(10) Ballinger, M. D.; Reed, G. H.; Frey, P. A. *Biochemistry* **1992**, *31*, 949−953.
(11) Wu, W.; Booker, S.; Lieder, K. W.; Bandarian, V.; Reed, G. H.; Frey, P. A. *Biochemistry* **2000**, *39*, 9561−9570.
(12) Miller, J.; Bandarian, V.; Reed, G. H.; Frey, P. A. *Arch. Biochem. Biophys.* **2001**, *387*, 281−288.
(13) Wu, W.; Lieder, K. W.; Reed, G. H.; Frey, P. A. *Biochemistry* **1995**, *34*, 10532−10537.

Scheme 3

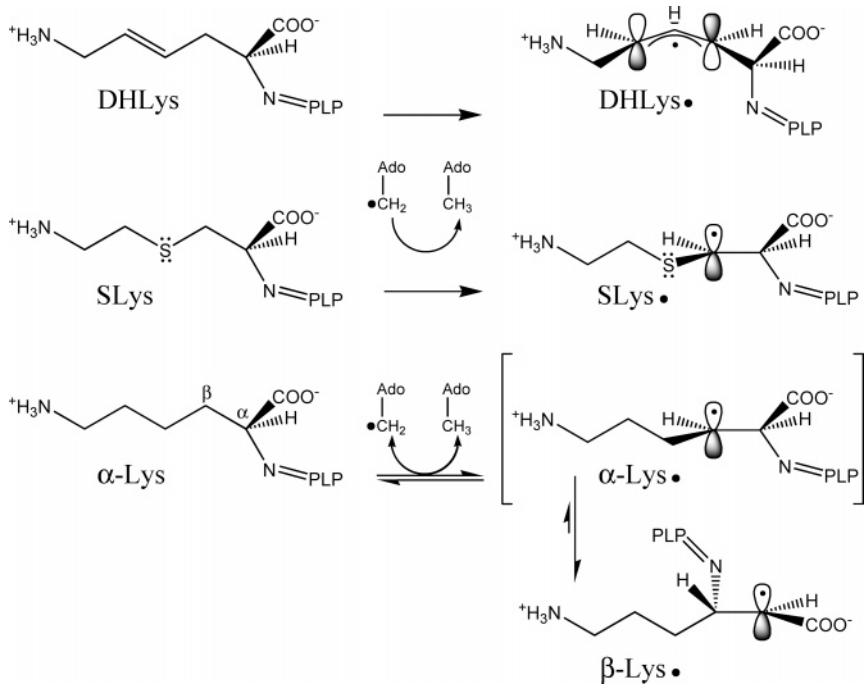

center enable the enzyme to minimize and even eliminate side reactions of highly reactive species.

Materials and Methods

Materials. Adenosine triphosphate (ATP), L-methionine, L-cysteine, *S*-adenosyl-L-methionine (SAM), L-4-thialysine hydrochloride, pyridoxal 5′-phosphate (PLP), adenylate kinase, creatine kinase, and phosphocreatine were purchased from Sigma. L-Lysine was obtained from FisherBiotech. Sodium dithionite and ammonium iron(II) sulfate were from Aldrich. L-[*methyl*-$^2H_3$]Methionine (minimum 98 atom % D) and L-[*methyl*-^{13}C]methionine (minimum 99 atom % ^{13}C) were purchased from Isotech Inc. (Miamisburg, OH). [5′-^{13}C]Adenosine (99 atom % ^{13}C) and [5′,5′-$^2H_2$]adenosine (98 atom % ^{2}H) were purchased from Omicron Biochemicals, Inc. (South Bend, IN). L-[U-^{14}C]Lysine was obtained from NEN Life Sciences Products. *trans*-4,5-Dehydrolysine was synthesized by W. Wu as described.[11] All other chemicals and reagents were of the highest purity and used as supplied.

Recombinant LAM from *Clostridium subterminale SB4* was expressed in *Escherichia coli* and purified under anaerobic conditions as described.[14,15] LAM was activated by incubation in 100 mM Epps buffer at pH 8.0 with 8.0 mM L-cysteine, 0.5 mM PLP, and 1.0 mM ferrous ammonium sulfate at 37 °C for 4 h in a Coy anaerobic chamber. Activity was assayed following a standard radiochemical procedure as described.[10]

Adenosine kinase was expressed and purified as described by Spychala et al.[16] SAM synthetase was expressed and purified as described by Markham et al.,[17] with some minor modifications. The activities of both adenosine kinase and SAM synthetase were assayed by HPLC methods.

SAM containing the ^{13}C or ^{2}H label in the methyl group was synthesized from ATP and L-[*methyl*-$^2H_3$]methionine or L-[*methyl*-^{13}C]-methionine with use of SAM synthetase-catalyzed reactions as described previously,[18] with minor modifications. SAM containing ^{13}C or ^{2}H label in the C5′-methylene group was synthesized from [5-^{13}C]adenosine or [5′,5′-$^2H_2$]adenosine in one-pot reactions catalyzed by adenosine kinase, adenylate kinase, creatine phosphokinase, and *S*-adenosylmethionine synthetase. First, [5′-^{13}C]ATP or [5′, 5′-$^2H_2$]ATP was produced in a reaction mixture containing 25 mM PIPES buffer at pH 7.0, 10 mM $MgCl_2$, 3.0 mM [5′-^{13}C]adenosine or [5′, 5′-$^2H_2$]adenosine, 0.3 mM ATP, 20 mM phosphocreatine, 10 IU adenosine kinase, 2000 IU adenylate kinase, and 2000 IU creatine phosphokinase in a total volume of 50 mL at 22 °C. The progress of the reaction was monitored by HPLC using a Hypersil SAX anion-exchange column (125 mm × 4.0 mm). The amount of unlabeled ATP in the product is minimized by using a much smaller amount of ATP to initiate the adenosine kinase and adenylate kinase reactions to form AMP and ADP, since ATP required for the complete phosphorylation is regenerated from ADP by the action of phosphocreatine kinase from the large excess of phosphocreatine. At the end of the reaction, the pH of the reaction mixture was raised to ∼7.4 by the addition of 6.0 mL of 1 M Tris-HCl at pH 8.0. Then, 3.5 mL of 1 M KCl, 1.3 mL of 1 M $MgCl_2$, 0.14 mL of 0.5 M EDTA at pH 8.0, 5.6 mL of β-mercaptoethanol, 3.0 mL of 100 mM L-methionine, 0.5 IU inorganic pyrophosphate, and ∼20 IU SAM synthetase were added. The reaction mixture was incubated at 22 °C for ∼5 h until all the ATP was converted to SAM as monitored by HPLC. The reaction was stopped by addition of HCl to 0.1 M, and the precipitated protein was removed by centrifugation. The pH of the supernatant fluid was adjusted to 5.0 with 1 M Tris and loaded onto a 2.5 cm × 15 cm CM-Cellulose column equilibrated with 1.0 mM sodium acetate buffer at pH 5.0. The column was washed with ∼3 column volumes of the equilibrating buffer until the A_{260} of the eluate was negligible. [5′-^{13}C]SAM or [5′,5′-$^2H_2$]SAM was eluted with 40 mM HCl. The solution of SAM was concentrated at reduced pressure and its pH adjusted to ∼5.0 with 1 M Tris. The incorporation of ^{13}C or ^{2}H was confirmed by mass spectrometric analysis of the synthesized SAMs, and their ability to fully support LAM activity was verified by enzymatic assay.

Preparation of ENDOR Samples. ENDOR samples were prepared under anaerobic conditions in a Coy anaerobic chamber. The purified

(14) Ruzicka, F. J.; Lieder, K. W.; Frey, P. A. *J. Bacteriol.* **2000**, *182*, 469−476.
(15) Petrovich, R. M.; Ruzicka, F. J.; Reed, G. H.; Frey, P. A. *J. Biol. Chem.* **1991**, *266*, 7656−7660.
(16) Spychala, J.; Datta, N. S.; Takabayashi, K.; Datta, M.; Fox, I. H.; Gribbin, T.; Mitchell, B. S. *Proc. Natl. Acad. Sci. U.S.A.* **1996**, *93*, 1232−1237.
(17) Markham, G. D.; Hafner, E. W.; Tabor, C. W.; Tabor, H. *J. Biol. Chem.* **1980**, *255*, 9082−9092.
(18) Magnusson, O. T.; Reed, G. H.; Frey, P. A. *Biochemistry* **2001**, *40*, 7773−7782.

LAM (~270 μM active sites) was activated by incubation with 10 mM L-cysteine in the presence of 0.42 mM PLP, 1.0 mM ammonium iron(II) sulfate, and 15% glycerol in 42 mM Epps buffer at pH 8.0 and 37 °C for 4 h. The activated enzyme was concentrated with Microcon 30 centrifugal filter devices (Millipore) so that the concentration of the enzyme active site was ~1.2 mM. The concentrated enzyme was quickly mixed with SAM ([*methyl*-^{13}C]SAM, [*methyl*-D_3]SAM, [5′-^{13}C]SAM, or [5′,5′-$^2H_2$]SAM), sodium dithionite, and L-lysine (L-4-thialysine or *trans*-L-4,5-dehydrolysine) in a 0.65 mL microcentrifuge tube. The mixed sample was rapidly transferred to an ENDOR sample tube and frozen in a cold isopentane bath immersed in liquid nitrogen. The time scale from mixing to sample freezing is from 1 to 1.5 min, sufficient time for equilibrium to be attained in the reaction of 0.9 mM LAM. In all samples, the concentration of the enzyme active site was ~0.9 mM; the concentrations of SAM, sodium dithionite, and lysine (or its analogue) were 3.0, 6.0, and 40 mM, respectively.

EPR and ENDOR Spectroscopy. Pulsed ENDOR spectra were collected on a spectrometer described earlier,[19] equipped with a helium immersion dewar for measurements at ~2 K. ENDOR measurements employed either the Mims or reMims pulse sequences ($\pi/2-\tau-\pi/2-T-\pi/2-\tau-$echo or $\pi/2-\tau1-\pi/2-T-\pi/2-\tau2-\pi-\tau1+\tau2-$echo, respectively; RF applied during interval T) for small hyperfine couplings[20] or the Davies pulse sequence ($\pi-T-\pi/2-\tau-\pi-\tau-$echo) for large couplings.[8]

For nuclei (N) of spin $I = {}^1/_2$ (^{13}C, ^{1}H, ^{31}P) interacting with an $S = {}^1/_2$ paramagnetic center, the first-order ENDOR spectrum for a single molecular orientation is a doublet with frequencies (ν_+/ν_-),

$$\nu_\pm = \nu_N \pm A/2 \quad (1)$$

where ν_N is the Larmor frequency and A is the orientation-dependent hyperfine constant. For nuclei with $I = 1$ (^{2}H and ^{14}N), the first-order ENDOR condition can be written:

$$\nu_\pm(\pm) = |\nu_N \pm \frac{A}{2} \pm \frac{3P}{2}| \quad (2)$$

where P is the orientation-dependent quadrupolar splitting.

For a nucleus with hyperfine coupling A, Mims pulsed ENDOR has a response R which depends on the product, $A\tau$, according to the equation

$$R \sim [1 - \cos(2\pi A\tau)] \quad (3)$$

This function has zeros, corresponding to minima in the ENDOR response (hyperfine "suppression holes"), at $A\tau = n$ ($n = 0, 1, ...$) and maxima at $A\tau = (2n + 1)/2$ ($n = 0, 1, ...$).[8,20] The "holes" at $A = n/\tau$ ($n = 1, 2, 3, ...$) can be adjusted by varying τ. However, the "central" ($n = 0$) hole at $\nu = \nu_N$ persists regardless. This can be of significance in distinguishing a tensor that is dominated by anisotropic interactions from one that is dominated by isotropic ones. The latter would never lead to ENDOR intensity near ν_N; the former does so for certain orientations, but the $\nu = 0$ Mims hole tends to diminish the differences between the two cases.

For states **1** and **−1**, we use the [4Fe-4S]$^+$ cluster as the paramagnetic probe. Its EPR signal has sufficient g anisotropy that orientation-selective ENDOR techniques can yield full hyperfine tensors for nuclei studied by ENDOR.[21−23] The very small dispersion of g values for the radicals studied here is not resolved within the intrinsic EPR line width, even at 35 GHz. Consequently, ENDOR spectra of nuclei hyperfine-coupled to a radical are an isotropic powder-averaged pattern. Analysis of these powder patterns yields distances between the radical center and spin-bearing nuclei, as well as bonding and orbital overlap properties, but not orientations relative to the g-frame.

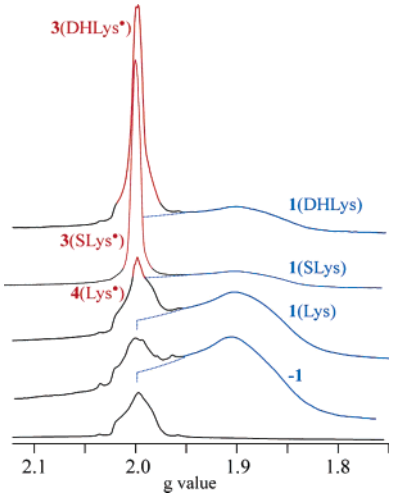

Figure 2. 35 GHz EPR of LAM with PLP, reduced in the presence of SAM and DHLys, SAM and SLys, SAM and Lys, or SAM only. Background signal from oxidized LAM(2+) sample with PLP only. Blue portions of spectra from reduced [4Fe-4S]$^+$ cluster (state **1**), red portions of spectra from DHLys, SLys (state **3**), and Lys (state **4**) radicals; background spectrum (black) from residual Mn^{2+}. Experimental conditions: T = 2 K; microwave power = 0.1 mW; modulation amplitude = 0.7 G (0.3 G for SLys); frequency = 34.952 GHz for DHLys, 35.030 GHz for SLys, 34.892 GHz for Lys, 35.092 GHz for SAM only, and 34.994 GHz for LAM(2+).

Results

EPR Measurements. Figure 2 presents 35 GHz EPR spectra of state **−1** (Scheme 2) and from the three turnover samples generated during one-electron reduction of LAM state **0** prepared with PLP-bound Lys, DHLys, or SLys. Each of the turnover samples exhibits a signal from the corresponding state **1**, a rhombic EPR spectrum from the [4Fe-4S]$^+$ cluster with g = [~2.0, 1.90, 1.85]. In addition, each shows a narrow $g = 2$ signal from the substrate/analogue radical of the corresponding state **3/4** that is in equilibrium with its state **1**. The relative areas of the two signals for a given sample reflect the relative populations of the states **1** and **3/4**. Included in the figure is a background spectrum from the nominally diamagnetic LAM with a [4Fe-4S]$^{2+}$ cluster and bound PLP only; it displays a signal from a Mn^{2+} impurity that also is observed in all the other spectra.

Distance from Substrate Radical to Adenosine-5′-Methyl-($^{13}C^{1,2}H_3$) in Intermediates 3 and 4. In the X-ray structure of LAM in state **0**, the distance between the β-carbon of the lysine substrate and the 5′-methylene carbon of SAM is 3.8 Å.[7] To assess changes in active-site geometry during catalysis, we have measured the distance in states **3** and **4** from the radical intermediates to the 5′-methyl of the deoxyadenosine generated by catalytic cleavage of SAM. This has been done by ^{13}C-labeling the 5′-position of the SAM ribose and measuring the distance from ^{13}C ENDOR spectra of the substrate radicals.

The spectra of the **3**(SLys•), **4**(Lys•), and **3**(DHLys•) states in Figure 3 all show a 5′-$^{13}CH_3$-Ado ν_+ peak which is absent in the spectra of the unlabeled samples (Supporting Information). The spectrum of **3**(DHLys•) has a somewhat smaller hyperfine

(19) Davoust, C. E.; Doan, P. E.; Hoffman, B. M. *J. Magn. Reson.* **1996**, *119*, 38−44.
(20) (a) Mims, W. B. In *Electron Paramagnetic Resonance*; Geschwind, S., Ed.; Plenum Press: New York, 1972. (b) Doan, P. E.; Hoffman, B. M. *Chem. Phys. Lett.* **1997**, *269*, 208−214.
(21) DeRose, V. J.; Hoffman, B. M. In *Methods in Enzymology*; Sauer, K., Ed.; Academic Press: New York, 1995; Vol. 246, pp 554−589.
(22) Hoffman, B. M.; Venters, R. A.; Martinsen, J. *J. Magn. Reson.* **1985**, *62*, 537−542.
(23) Hoffman, B. M.; Martinsen, J.; Venters, R. A. *J. Magn. Reson.* **1984**, *59*, 110−123.

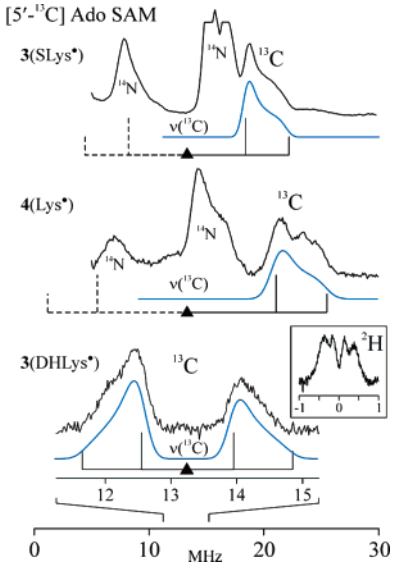

Figure 3. 35 GHz ^{13}C ENDOR of **3**(SLys•), **4**(β-Lys•), and **3**(DHLys•). Inset: ^{2}H ENDOR from sample with DHLys and [5′,5′-$^{2}H_2$]-SAM. Baseline from unlabeled sample has been subtracted. Spectra collected at peak of radical EPR spectrum in each sample (g = 2.002). Simulations shown in blue below spectra. Experimental conditions: T = 2 K; repetition rate = 100 Hz for **3**(SLys•), 200 Hz for **4**(β-Lys•) and **3**(DHLys•) ^{13}C, and 50 Hz for **3**(DHLys•) ^{2}H; RF pulse length = 60 μs. For **3**(SLys•) ^{13}C Davies pulse sequence, MW pulse lengths = 80, 40, and 80 ns, ν_{MW} = 34.821 GHz; for **4**(β-Lys•) Davies pulse sequence, MW pulse lengths = 80, 40, and 80 ns, ν_{MW} = 34.711 GHz; for **3**(DHLys•) ^{13}C ReMims pulse sequence, MW pulse length = 32 ns, τ = 248 ns, ν_{MW} = 34.691 GHz; for **3**(DHLys•) ^{2}H Mims pulse sequence, MW pulse length = 52 ns, τ = 452 ns, ν_{MW} = 34.682 GHz. Simulation parameters: for **3**(SLys•), T = 2.5 MHz, A_{iso} = 12.7 MHz, ENDOR line width = 1.0 MHz; for **4**(β-Lys•), T = 2.9 MHz, A_{iso} = 18.5 MHz, ENDOR line width = 1.8 MHz; for **3**(DHLys•), T = 0.6 MHz, A_{iso} = 2 MHz, ENDOR line width = 0.3 MHz, Mims suppression simulated with τ = 200 ns.

coupling and also shows the ν_- peak (eq 1). We have simulated the spectra (Figure 3) and found that each is describable by a hyperfine tensor that is dominated by the isotropic hyperfine coupling, A_{iso}, and accompanied by an axial anisotropic interaction, $\mathbf{T} = [-T,-T,+2T]$. The splitting between the maximum-intensity (perpendicular) feature of the two branches of such spectra is $A_\perp = (A_{iso} - T)$, the "parallel" splitting is $A_\parallel = (A_{iso} + 2T)$, and the width of an individual branch is $3T/2$. The experimental hyperfine tensors give $A_{iso} = +18.5$ MHz, $T = +2.9$ MHz for **4**(Lys•), $A_{iso} = +12.7$ MHz, $T = +2.5$ MHz for **3**(SLys•), and $A_{iso} = +2.0$ MHz, $T = +0.6$ MHz for **3**(DHLys•). The shapes of the patterns show that A_{iso} and T have the same sign; in the next paragraph we justify the choice of the positive sign.

The anisotropic interaction is the sum of two axial components. One is a tensor, $\mathbf{T}_{n-loc}$, that arises from the dipolar interaction between the 5′-$^{13}CH_3$ nuclear spin and the electron spin of the radical. It is characterized by a parameter, T_{n-loc}, which is necessarily positive; in the point-dipole approximation it is related to the electron−nuclear distance through the expression

$$r_{(Fe-N)} = [g_e\beta_e g_N\beta_N/T_{n-loc}]^{1/3} \qquad (4)$$

where the constants have their usual meanings and the nuclear g factors, g_N, have previously been tabulated.[24] The second tensor, $\mathbf{T}_{loc}$, arises from interaction of the ^{13}C with spin density delocalized into the sp^3 orbital of a methyl C−H/D bond (Supporting Information), as does A_{iso}. Both A_{iso} and T_{loc} are of the same sign (positive or negative), with well-defined relative magnitudes (Supporting Information).

The decomposition of **T** into local and nonlocal terms (Supporting Information) shows that $T_{n-loc} > T_{loc}$ for **3**(SLys•) and **3**(DHLys•). As a result, T has the positive sign of T_{n-loc}. The finding that A_{iso} and T have the same sign thus shows that A_{iso}, and hence T_{loc}, are also positive. For **4**(Lys•), $T_{n-loc} < T_{loc}$, so it is possible that A_{iso}, T_{loc}, and T could all be negative. However, we see no physical reason for A_{iso} to have the opposite sign in **4**(Lys•), and we drop this option.

The large isotropic ^{13}C couplings indicate that there is significant spin delocalization onto the 5′-$^{13}CH_3$ probe from the substrate-derived radical, which implies that, in each intermediate, the 5′-methyl of the 5′-Ado generated by H-atom transfer to the 5′-$^{13}CH_2$ radical of state **2** is in contact with the substrate radical created by this reaction. The distance from the radical spin to the ^{13}C, as calculated from T_{n-loc} and eq 4, is of limited value as the point-dipole approximation breaks down at short distances, but the value obtained, $r \approx 2.4$ Å for **4**(Lys•) and **3**(SLys•), is of heuristic value and supports the conclusion that the $^{13}CH_3$-Ado is at least in van der Waals contact with the radical (Supporting Information). For **3**(DHLys•), analysis[25] requires that one take into account the 50/50 partitioning of the spin density onto the β- and δ-carbons. Such an analysis yields a distance $r(^{13}C-C_{\beta,\delta}) \approx 3.4$ Å, again supporting the conclusion.

The magnitude of the ^{13}C coupling correlates with the extent of orbital overlap between the radical and the 5′-$^{13}CH_3$-Ado: the contact thus must be better in **4**(Lys•) (A_{iso} = 18.5 MHz) than in **3**(Slys•) (A_{iso} = 12.7 MHz). The isotropic coupling for 5′-$^{13}CH_3$-Ado of **3**(DHLys•), A_{iso} = 2 MHz, is noticeably smaller than for the other two intermediates.[26] However, this coupling nonetheless is large enough to indicate that the 5′-$^{13}CH_3$-Ado of **3**(DHLys•) also is in van der Waals contact with its radical. We suggest that A_{iso} is reduced primarily because the close intermolecular contact involves the intervening γ-CH of DHLys•, which carries negligible spin density;[11] the smaller $A_{iso}(^{13}C)$ measured for the interaction with **3**(DHLys•) may further reflect poorer orbital overlap. As illustrated by Scheme 3, in the case of **3**(DHLys•), formation of the allyl radical significantly distorts the carbon backbone relative to the natural substrate radical, α-Lys•.

The 5′-methylene of SAM also was deuterated (5′-C$^2H_2$), and ^{2}H spectra were collected from **3**(SLys•) and **3**(DHLys•); the EPR spectrum of **4**(Lys•) was too weak to give satisfactory ^{2}H spectra. The **3**(DHLys•) intermediate gives the ^{2}H spectrum shown in Figure 3, after subtraction of background signals from $\Delta m = \pm 2$ transitions of ^{14}N. The spectrum shows a pair of broad outer features whose maximum splitting is ~0.8 MHz and a pair of sharper inner features split by 0.3 MHz. The outer features must be associated with a relatively strongly coupled ^{2}H. The inner features could be reasonably interpreted in either of two ways: as a signal from more weakly coupled ^{2}H or as part of the broader signal. In either case, the well-defined features of the spectrum suggest that the 5′-C$^2H_2$^{1}H-Ado group

(24) Weil, J. A.; Bolton, J. R.; Wertz, J. E. *Electron Paramagnetic Resonance: Elementary Theory and Practical Applications*; John Wiley & Sons: New York, 1994.
(25) DeRose, V. J.; Liu, K. E.; Lippard, S. J.; Hoffman, B. M. *J. Am. Chem. Soc.* **1996**, *118*, 121−134.
(26) Although much larger than that to the methyl group of Met in this state.

is locked into a relatively well-defined orientation at the low temperature of measurement. If the methyl were also locked at ambient temperature, then the C−^{1}H bond that forms when the 5′-CD_2-Ado radical abstracts an ^{1}H-atom from substrate would be directed at the resulting substrate radical, but of course it would be invisible in the ^{2}H ENDOR. However, this methyl undoubtedly undergoes three-fold rotation at ambient, and thus the three rotamers must have equilibrated before the sample was frozen. As a result, the C−H bond that forms has become two-thirds occupied by ^{2}H, and we may assign the large observed ^{2}H coupling to the C−H bond that is directed at the radical and is involved in accepting and donating an H-atom during catalysis. In the catalytic intermediate, it would have the strongest overlap with the odd electron on the substrate radical and thus the largest coupling.

We favor the interpretation of the spectrum as arising from coupling to multiple deuterons, one ^{2}H with large coupling and one or more with small couplings; the one-deuteron model is discussed in the Supporting Information. When the spectrum is interpreted as arising from more than one ^{2}H, the narrow ^{2}H signal may represent the combined response of the other two ^{2}H sites, which are indistinguishable in this "reactive" geometry, or it may represent a second ^{2}H, with the third having a yet smaller coupling and unresolved signal. The narrow feature was assumed to be solely dipolar, with no isotropic component, as found elsewhere; [27] it was reproduced with $T \approx +0.2$ MHz. The larger ^{2}H coupling was assumed to have a positive A_{iso} to match the sign for ^{13}C, and $T > 0$, as T has no local component for a ^{2}H nucleus. Simulations were performed as T and A_{iso} were jointly varied within the constraint that they match the overall width of the spectrum, $[A_{iso} + 2T]$. Two distinct regimes of solutions emerged: in one, $0.3 \lesssim T \lesssim 0.6$ MHz, in which case $0.55 \gtrsim A_{iso} \gtrsim 0.20$ MHz; in the other, $T \approx 0.85$ MHz and $A_{iso} \approx 0$.

Bonding considerations allow us to select preferred values. The presumed mechanism for the introduction of the large ^{13}C and ^{2}H isotropic couplings is direct overlap between the methyl C−D bond and the odd-electron π orbital of DHLys•, leading to partial delocalization of the spin into that bond. It is easy to show (see Supporting Information) that, when the radical spin density is delocalized into a covalent bond between an H-atom and an sp^3 hybrid orbital of carbon, one expects the isotropic ^{1,2}H coupling and ^{13}C coupling to have the same sign and be related by $A_{iso}(^2H) \approx [3/(2(g_H/g_D = 6.51))]A_{iso}(^{13}C)$. For **3**(DHLys•), $A_{iso}(^{13}C) = +2$ MHz would then correspond to $A_{iso}(^2H) \approx +0.46$ MHz, well within the acceptable range; for this value the fit gives $T(^2H) \approx 0.4$ MHz. Our reason for disfavoring the one-deuteron model (Supporting Information) is that it gives $A_{iso}(^2H) = 0.17$ MHz, which is significantly lower than the predicted value. In either case, the delocalization of spin into a 5′-Ado-methyl C−H bond, as demonstrated by the isotropic hyperfine couplings to *both* ^{13}C and ^{1,2}H, definitively establishes that the 5′-methyl is in contact with the radical.

In contrast to the above, ^{2}H ENDOR spectra of **3**(SLys•) did not disclose *any* ^{2}H signal over a background of $\Delta m = \pm 2$ transitions from ^{14}N. Given the large coupling to the Ado-(5′-^{13}C), $A_{iso}(^{13}C) = 12.7$ MHz, the ^{2}H coupling to the adjacent (5′-CD) bond should have a value of roughly $A_{iso}(^2H) \approx [3/(2 \times 6.51)]A_{iso}(^{13}C) \approx 2.9$ MHz, and this should have been seen readily. We suggest that the absence of the signal reveals that the deuterons of the 5′-C$^2H_2$ have "washed out" during the reaction: although SLys is a poor substrate, it does react, and it took 1−1.5 min to freeze the sample. Apparently, during that time, the enzyme cycled enough times to dilute the C−^{2}H to below detectability.

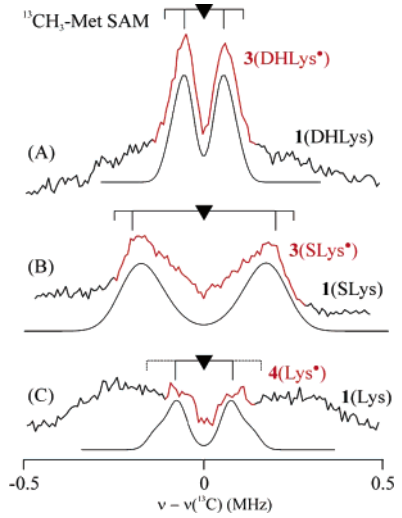

Figure 4. 35 GHz ^{13}C Mims ENDOR of LAM(+1) + (*methyl*-^{13}C)-methionine-SAM + PLP + (DHLys, Lys, or SLys). Spectra collected at peak of radical EPR spectrum in each sample ($g = 2.002$). Red portions of spectra from interaction of (A) DHLys, (B) SLys (state **3**), and (C) Lys (state **4**) radicals with ^{13}C label. Background signals in (A) and (C) are from interaction of unpaired cluster spin (state **1**) with ^{13}C label of coordinated SAM. Experimental conditions: $T = 2$ K; ν_{MW}(+DHLys) = 34.695 GHz; ν_{MW}(+Lys) = 34.834 GHz; ν_{MW}(+SLys) = 34.761 GHz; MW pulse length = 52 ns; $\tau = 500$ ns; RF pulse length = 40 μs (+DHLys,-Lys), 60 μs (+SLys); repetition rate = 200 Hz. Simulation parameters: Mims suppression simulated with $\tau = 500$ ns; (A) $T = 0.11$ MHz, ENDOR line width = 0.05 MHz; (B) $T = 0.3$ MHz, $A_{iso} = 0.1$ MHz, ENDOR line width = 0.12 MHz; (C) $T = 0.16$ MHz, ENDOR line width = 0.05 MHz.

Distances from Substrate Radical to Methionine-*$^{13}CH_3$* in Intermediates 3 and 4. In the major conformation of LAM state **0**, the distance between the β-carbon of the lysine substrate and the methyl carbon of the methionine of SAM is approximately 5 Å.[7] To look for changes in this distance upon cleavage of SAM during formation of the **3** and **4** intermediate states, the Met-methyl has been ^{13}C-labeled and ENDOR spectra of the substrate radicals in intermediate states **3** and **4** have been collected. Figure 4 presents ^{13}C ENDOR spectra from states **3**(DHLys•), **3**(SLys•), and **4**(Lys•) in samples prepared with $^{13}CH_3$-SAM. Each spectrum contains a broad background ^{13}C signal associated with the **1** state, as is most clearly seen for **4**(Lys•); this reflects a ^{13}C ENDOR response from the underlying EPR signal from the [4Fe-4S]$^+$ cluster in **1**, interacting with the cluster-bound $^{13}CH_3$ SAM. Superimposed on this background, all three spectra have a narrow, sharp ^{13}C doublet that results from ENDOR of the substrate radical in states **3**/**4**. The hyperfine splittings of these doublets, which are over an order of magnitude smaller than those from the 5′-$^{13}CH_3$-Ado, reflect a through-space dipolar interaction of the radical with the ^{13}C-Met that is liberated by cleavage of SAM and that remains bound to the cluster. The sharp ^{13}C doublet associated with **4**(Lys•) is barely visible on the more intense broad signal from **1**(Lys), but comparisons with spectra from state −**1** itself confirm its presence.

Given the ~5.0 Å distance between the cluster-bound $^{13}CH_3$-Met-methyl and the β-carbon of substrate in the X-ray structure

(27) Warncke, K.; Utada, A. S. *J. Am. Chem. Soc.* **2001**, *123*, 8564−8572.

Table 1. Distances to the Radical in Various LAM States

		distance from R to:		
state	R	^{13}C-met	5′-^{13}C	^{31}P (PLP)
0[a]	C_α, C_β (Lys)	5.5, 5.2 Å	4.2, 3.8 Å	6.4, 6.7 Å
3	$C_{\beta,\delta}$ (DHLys•)	∼5.5 Å	van der Waals	3.6 Å
	C_β (SLys•)	≥4.1 Å	van der Waals	4.3 Å
4	C_α (β-Lys•)	∼5 Å	van der Waals	

[a] Reference 7.

of state **0**,[7] the small coupling of $^{13}CH_3$-Met to the spin of the radical (Figure 4**)** was to be expected (eq 4). The spectrum of **4**(Lys•) can be simulated by treating the radical spin as a point dipole with coupling parameter $T = 0.16$ MHz, determined from the splitting between the maxima in the spectrum. Equation 4 gives the corresponding distance between the α-carbon radical and the cluster-bound $^{13}CH_3$-SAM, $r \approx 5.0$ Å. For **3**(DHLys•), we can incorporate the delocalization of the electron spin onto C_β and C_δ by a published approach,[25] which gives $r(^{13}C-C_{\beta,\delta}) \approx 5.5$ Å. Comparison with the corresponding distance in the X-ray structure of state **0** suggests there is little change in this distance in states **3** and **4** (Table 1). In fact, little motion is required by our proposal that the sulfur of methionine becomes the sixth ligand to the unique iron upon reductive cleavage of SAM.[3] The non-coordinating S(Se)−Fe distance in the structure of state **0** is 3.15 Å, whereas the S−Fe bonding distance in states **2**−**4** would be nearly 3 Å.[28] For **3**(SLys•), an isotropic coupling $A_{iso} \geq 0.1$ MHz is required for a satisfactory simulation; in the fits, the accompanying point-dipole coupling is $T \leq 0.3$ MHz, which corresponds to a distance from the radical to ^{13}C Met $r \geq 4.1$ Å.

Distances of Substrate Radical to PLP-*^{31}P*. That PLP is involved in an aldimine linkage to the β-lysine radical of **4**(Lys•) was demonstrated previously by electron spin−echo envelope modulation (ESEEM) spectroscopy on the deuterium-labeled cofactor.[29] A distance of <3.5 Å from the radical center to a ^{2}H at C4′ of PLP was reported. We have used ^{31}P Mims ENDOR measurements to examine the proximity of the phosphate group of PLP to the radical centers of **3**(SLys•) and **3**(DHLys•). The EPR signal of **4**(Lys•) is at least an order of magnitude weaker than those of the substrate-analogue radicals, and ^{31}P ENDOR signals were not detected from this signal.

Figure 5 shows ^{31}P Mims ENDOR spectra from states **3**(SLys•) and **3**(DHLys•). These spectra are similar to the ^{2}H ENDOR spectra of Figure 3 in that they show two types of ^{31}P features centered on the ^{31}P Larmor frequency: a doublet of sharp peaks split by $A(^{31}P) \approx 0.13$ MHz for **3**(DHLys•) and 0.20 MHz for **3**(SLys•) is flanked by broad shoulders with total breadth of approximately 1 MHz. As with the ^{2}H spectra, the ^{31}P spectra of Figure 3 may be interpreted in terms of either a single ^{31}P, for which the spectrum is distorted by the effects of Mims suppression, or two conformations of the PLP. Parallel studies with deuterated PLP will help to distinguish these possibilities. Within the one-^{31}P interpretation, the ^{31}P Mims ENDOR patterns for **3**(DHLys•) and **3**(SLys•) both can be well-simulated with $A_{iso} = 0.43$ MHz, $T = 0.59$ MHz for **3**(DHLys•) and $A_{iso} = 0.19$ MHz, $T = 0.41$ MHz for **3**(SLys•) (Figure 5). Only a tiny electron-spin density at the ^{31}P nucleus, $\rho = 3 \times 10^{-5}$,

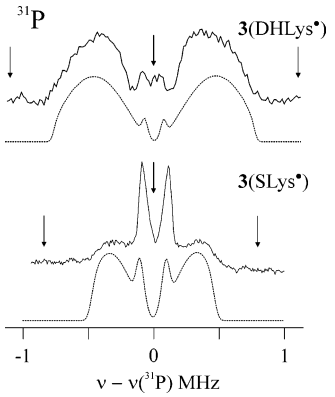

Figure 5. 35 GHz ^{31}P ENDOR spectra of **3**(DHLys•) and **3**(SLys•), collected at peak of radical EPR spectrum in each case ($g = 2.002$). Simulation shown with dashed line. Conditions: $T = 2$ K; Mims pulse sequence, MW pulse lengths = 52 ns, RF pulse length = 60 μs; repetition rate = 100 Hz; for **3**(DHLys•), $\tau = 452$ ns, $\nu_{MW} = 34.483$ GHz; for **3**(SLys•), $\tau = 600$ ns, $\nu_{MW} = 34.809$ GHz. Simulation parameters (Mims suppression simulated with experimental τ): for **3**(DHLys•), $T = 0.59$ MHz, $A_{iso} = 0.43$ MHz, ENDOR line width = 0.3 MHz; for **3**(SLys•), $T = 0.41$ MHz, $A_{iso} = 0.19$ MHz, ENDOR line width = 0.06 MHz.

is required to produce the observed A_{iso}. In principle, the anisotropic ^{31}P interaction is a sum of local and nonlocal contributions, as for the ^{13}C probe, but it is easy to show that the local contribution can be ignored. Inserting T into eq 4 then gives a radical-to-^{31}P distance of $r = 4.3$ Å for **3**(SLys•). Applying the two-site-radical treatment to the **3**(DHLys•) allyl radical with P equidistant from C_β and C_δ gives $r(^{31}$P-radical$) = 3.6$ Å. A detailed analysis in terms of two conformations is not warranted by the data, but it too would suggest a close approach in at least one of the conformations.

^{14}N ENDOR of Intermediates. Davies ENDOR spectra from **3**(DHLys•), **3**(SLys•), and **4**(Lys•) radicals reveal ^{14}N ENDOR signals in the 5−20 MHz range (Figure 6). The **3**(DHLys•) spectrum consists of two peaks that have a separation too large to arise from a quadrupole splitting but much smaller than $2\nu(^{14}N)$, which would separate the $\nu_\pm$ branches of a single nitrogen (eq 3). Thus, they are assigned as the ν_+ branches of two different ^{14}N nuclei that have unresolved quadrupole splittings. As shown in Figure 6, the two signals are well simulated with hyperfine interactions dominated by a large isotropic component: $A_{iso} = 7.5$ MHz (N_1), 17.7 MHz (N_2).[30]

The ^{14}N ENDOR spectra of **3**(SLys•) and **4**(Lys•) also show two ^{14}N peaks, but in this case they are separated by $2\nu(^{14}N)$ and thus are assigned as the ν_+ and ν_- branches of a single ^{14}N. Again, the hyperfine coupling is predominantly isotropic, $A_{iso} = 23-25$ MHz for both states.[31] The presence of signals from two different nitrogens for the **3**(DHLys•) radical, and only one for **4**(Lys•) and **3**(SLys•), may be explained with reference to the structures shown in Figure 7. For the **3**(DHLys•) allyl radical, the spin-bearing $2p\pi$ orbitals of C_β and C_δ each are separated by two bonds from the ^{14}N at the two ends of the molecule, which give the two observed signals. The radical centers of **3**(SLys•) and **4**(Lys•) are separated by two bonds from the closest nitrogen, but by four and five bonds, respectively, from the second ^{14}N of the molecule. Therefore, only the nearer ^{14}N is observed.

(28) Cosper, N. J.; Booker, S. J.; Ruzicka, F.; Frey, P. A.; Scott, R. A. *Biochemistry* **2000**, *39*, 15668−15673.
(29) Ballinger, M. D.; Frey, P. A.; Reed, G. H.; LoBrutto, R. *Biochemistry* **1995**, *34*, 10086−10093.
(30) The anisotropic interactions are $T = [2,1,-3]$ MHz for N_1 and $[-1.7, -1.7, 3.4]$ MHz for N_2.
(31) Axial anisotropic interactions: $T = 2.5$ MHz for Lys; $T = 2.4$ MHz for SLys.

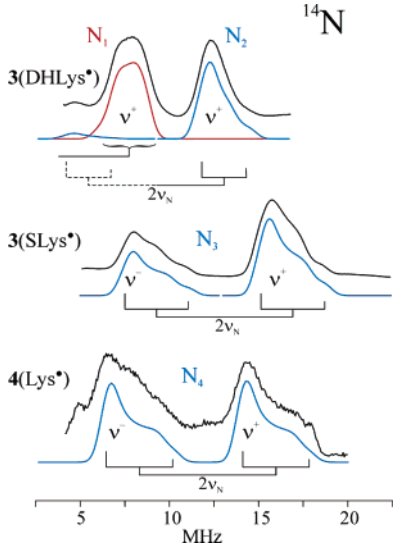

Figure 6. 35 GHz Davies ENDOR of LAM(+1) + SAM + PLP + (DHLys, SLys, or Lys). Spectra collected at peak of radical EPR spectrum in each sample ($g = 2.002$). Simulations shown below experimental spectra. Experimental conditions: $T = 2$ K; Davies pulse sequence, MW pulse lengths = 80, 40, and 80 ns, repetition rate = 200 Hz (100 Hz for **3**(SLys•)), RF pulse length = 60 μs; ν_{MW}(**3**(DHLys•)) = 34.724 GHz; ν_{MW}(**3**(SLys•)) = 34.808 GHz; ν_{MW}(**4**(β-Lys•)) = 34.750 GHz. Simulation parameters: for N_1, $A = [9.5, 8.5, 4.5]$, $P = [0.3, 0.3, -0.6]$, ENDOR line width = 0.8 MHz; for N_2, $A = [16, 16, 21]$, $P = [0.2, 0.2, -0.4]$, ENDOR line width = 0.8 MHz; for N_3, $A = [22.6, 22.6, 29.7]$, $P = [0.2, 0.2, -0.4]$, ENDOR line width = 0.8 MHz; for N_4, $A = [20.5, 20.5, 28]$, $P = [0.15, 0.15, -0.3]$, ENDOR line width = 0.8 MHz.

Discussion

Our goal in this work has been to study the arrangements and movements of the active-site components of LAM during the course of the α-lysine-to-β-lysine isomerization (Scheme 2). We have studied state **3** through ENDOR examination of radicals generated from the substrate analogues, *trans*-4,5-dehydrolysine and 4-thialysine, as paramagnetic probes; to study state **4** we used the β-lysyl radical in its equilibrium concentration. Hyperfine couplings of the radicals to ^{13}C and ^{2}H nuclei in the Met and 5′-Ado components of SAM allow us to see how these fragments move upon cleavage of SAM and formation of the substrate radical. Combined with a measurement of distances to an adenosyl radical analogue[9], these allow us to "triangulate" movements of active-site components as the enzyme traverses its reaction cycle. We have also measured ^{31}P couplings to the PLP phosphate, demonstrating the linkage between the PLP and substrate, and ^{14}N couplings to the nitrogens of the substrate.

To put the current work in context, we will briefly summarize studies of states "**0**", "−**2**", −**1**, **1**, and **2** in Scheme 2, and then discuss the current results for states **3** and **4**.

States 1 and Prior. In all members of the radical-SAM superfamily studied to date, enzyme activation begins with reduction of a $[4Fe\text{-}4S]^{2+}$ cluster. In the LAM cycle, this corresponds to one-electron reduction of state **0** to state **1** in Scheme 2. In the resulting equilibrium distribution of LAM intermediates that form with the native substrate, Lys, state **1**(Lys) is dominant and is readily accessible to ENDOR study through the paramagnetic $[4Fe\text{-}4S]^{+}$ ($S = {}^1/_2$) cluster. Previous ^{15}N,^{17}O ENDOR experiments on state −**1**[3] (state **1** without the presence of substrate) paralleled earlier work on PFL-AE[1,2] in demonstrating that the cofactor binds to the labile site of the [4Fe-4S] cluster through chelation by the amine nitrogen and a carboxylate oxygen of the methionine component of SAM. In addition, ^{13}C and ^{2}H labeling of the SAM sulfonium methyl group enabled ENDOR experiments that demonstrated that the sulfonium sulfur interacts with the [4Fe-4S] cluster,[32] gave information about the disposition of the Met-methyl relative to the cluster, and allowed us to propose a mechanism for the cleavage of SAM that results from its reduction by the cluster.[3] The presence of substrate has no effect on the ENDOR spectra (not published), and thus states −**1** and **1** are structurally equivalent at the cluster. The $[4Fe\text{-}4S]^{2+}$ cluster of the enzyme in state −**2** (or **0**) is diamagnetic, and this state is not directly accessible to EPR and ENDOR experiments. We nonetheless disclosed chelation of the methionyl amino acid of SAM to the $[4Fe\text{-}4S]^{2+}$ cluster of state −**2**, through cryoreductive generation of the $[4Fe\text{-}4S]^{+}$ cluster ($S = {}^1/_2$) with all active-site components locked in the conformation of the parent −**2** state.[3] These earlier ENDOR experiments showed that SAM binds to the [4Fe-4S] cluster with the same geometry in states −**2** and −**1** (or **0** and **1**). We extrapolate these observations to infer that the methionine amino acid remains coordinated to the unique Fe site of the cluster throughout the LAM enzymatic cycle.

These studies have been confirmed by the recent X-ray structure determination of LAM state **0**.[7] Of significance here, the X-ray structure provides a firm foundation for the present study of active-site motions during catalysis.

State 2. It is believed that cluster reduction is followed by reductive cleavage of SAM to form the highly reactive 5′-deoxyadenosyl radical (5′-Ado•) (Scheme 2). EXAFS analysis of a selenium derivative of SAM[28] demonstrated that cleavage of Se−SAM forms SeMet, which binds to the Fe−S cluster, and our ENDOR study led us to propose this binding as part of the mechanism for SAM cleavage.[3] The 5′-Ado• radical is too reactive to be observed, but Magnusson et al.[9] used the SAM analogue *S*-3′,4′-anhydroadenosylmethionine (anSAM) to produce a state **2** that contains the stable analogue of the 5′-Ado radical, 5′-deoxy-3′,4′-anhydroadenosine-5′-yl (anAdo•). ^{13}C and ^{2}H labeling of C2 (α-carbon) of lysine and the methyl C of anSAM was employed to examine the distance between the anAdo• radical and the lysine and Met components. These experiments confirmed the well-accepted idea that 5′-Ado• is formed by cleavage of SAM and indicated that the distance from the anAdo• to the lysine β-carbon of **2** is essentially the same as that from the 5′-methyl of SAM in **0**.

State 3. When LAM is reduced in the presence of the substrate analogues, SLys or DHLys, the system advances to states **3** that contain a stable substrate-analogue radical, denoted respectively **3**(SLys•) and **3**(DHLys•). The β-carbon SLys• radical, which is stabilized by the adjacent S, is a strict analogue for the β-carbon radical of α-Lys•. The DHLys• allylic π radical of **3**(DHLys•) has 50% of its spin on the β-carbon and 50% on the δ-carbon, and thus the correspondence is less strict.

When **3**(SLys•) and **3**(DHLys•) are prepared with [5′-^{13}C]-SAM, the ^{13}C ENDOR spectra from the DHLys• and SLys• radicals show large *isotropic* hyperfine couplings to the [5′-^{13}C]-Ado that was produced by H-atom transfer from the corresponding substrate to [5′-^{13}C]-Ado• of the (unobserved)

(32) Reanalysis of the methionine ($^{13}CH_3$) ENDOR data reveals an isotropic hyperfine coupling which indicates that the S of Met does interact with the cluster in LAM, as well as in PFL-AE.

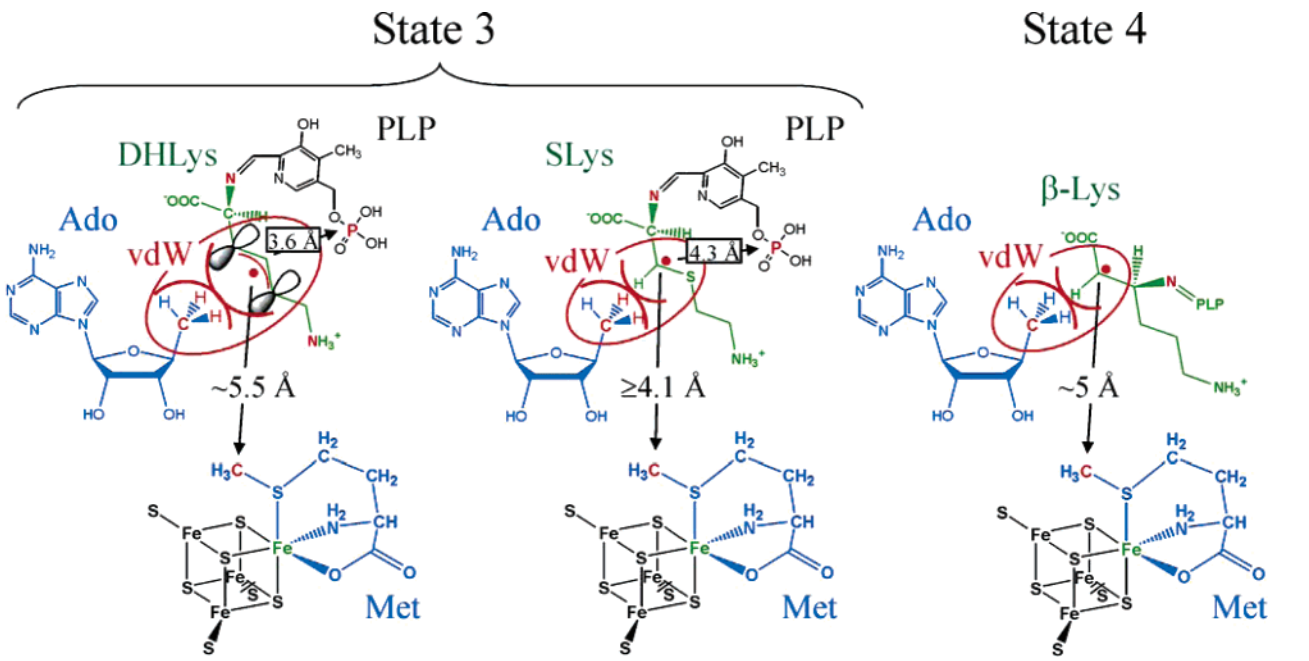

Figure 7. Arrangement of reactive components in LAM active site as determined from 35 GHz ENDOR experiments. Atoms detected interacting with the radical centers are colored red.

state **2**. Such a coupling must arise from direct orbital overlap of the radical and 5′-methyl of 5′-Ado and indicates that there is direct van der Waals contact between the substrate radical of state **3** and the 5′-Ado methyl group. This is confirmed by the semiquantitative analysis of the large dipolar coupling (*T*) (Supporting Information). Comparison with the X-ray structure of LAM state **0**[7] suggests that the 5′-carbon of 5′-Ado and substrate have moved ∼0.5−1 Å closer as the enzyme has advanced from state **0** to state **3** of the catalytic cycle. The ENDOR results for state **2** suggest that this motion does not occur upon cleavage of SAM to form **2**, as the distance from the anAdo radical in the analogue of **2** remains approximately that seen by X-rays for state **0**.[9] Thus, it would appear that the substrate-to-5′-Ado• H-atom transfer that then generates **3** is enabled by a structural fluctuation in state **2**, and that **3** is the first state with a (relatively) stable active-site geometry that includes van der Waals contacts between 5′-Ado (the methyl group) and substrate (radical). The sharp ^{2}H ENDOR spectra from the 5′-C^{2}H$_{2}$^{1}H-methyl group that forms when 5′-Ado is 5′-deuterated further discloses that the contact between 5′-methyl and substrate radical occurs with an extremely well-defined geometry, most likely with a single, most-stable methyl group rotamer. Indeed, this finding suggests an impressive example of enzymatic evolutionary design whereby the H-atom transfer is facilitated because the reacting partners (the methyl group and the radical center) are constrained to adopt a geometry that is optimized for reaction through interactions with the enzyme pocket.

The large couplings of the 5′-methyl-Ado to the SLys• radical, for which the spin density is concentrated on the β-carbon as with α-Lys•, indicates that the methyl group is in contact with the β-carbon from which the H-atom was abstracted. This is consistent with the view that direct contact of the odd electron of the 5′-CH$_2$-Ado radical and a β-CH of substrate is central to the efficiency of H-atom transfer in this reaction. The ^{13}C-methyl isotropic coupling to the DHLys• radical is large enough to require van der Waals contact between the radical and the 5-methyl of 5′-Ado, but A_{iso}(^{13}C) is roughly 6-fold smaller than that for SLys•. If the geometries of the 5′-Ado−substrate contact were the same in **3**(SLys•) and **3**(DHLys•), then the difference in spin density at the β-CH of substrate, ∼100% in **3**(SLys•) and 50% in β **3**(DHLys•), would account for only a factor of ∼2. The additional decrease suggests to us that the geometry of the contact is somewhat distorted in **3**(DHLys•).

ENDOR studies of **3**(SLys•) and **3**(DHLys•) prepared with ^{13}CH$_3$-SAM show small ^{13}C couplings which indicate that the radical center of the substrate analogue is ∼5 Å from the methionine methyl carbon, consistent with the X-ray structure of state **0**.

The analyses of the ^{31}P ENDOR measurements give an isotropic ^{31}P coupling in state **3**, which is remarkable in that the distances from the spin-bearing carbons of the analogue radicals to ^{31}P are approximately 7 Å in the crystal structure of state **0**, and no isotropic coupling would be expected at this distance. In addition, the currently preferred analysis in terms of a single conformation suggests that the PLP phosphate group lies moderately close to the radical centers in both **3**(DHLys•) and **3**(SLys•), less than ∼4.5 Å. The ENDOR analysis thus raises the possibility that the isomerization process may involve a significant movement of the PLP phosphate toward the radical site; such a change could also involve motion of the Ado fragment. This possibility will be tested by future ENDOR studies with samples that are ^{2}H labeled in PLP and in the Ado moiety of SAM.

The information regarding the relative positioning of the SAM components and substrate radical of state **3** leads to a model in which the reactive components of **3** are arranged as shown in Figure 7. After cleavage of SAM, the 5′-Ado• radical of state **2** adopts a conformation in which the reactive C5′ carbon contacts the location on the substrate from which the H-atom is to be abstracted, and this close contact persists once the H-atom has been transferred to generate state **3**.

State 4. The protein samples used in these experiments were allowed to equilibrate so as to allow each of the reactive species

in the reactive cycle shown in Scheme 2 to reach its equilibrium concentration. With Lys as substrate, only a small concentration of a radical species accumulates, assigned as the β-lysine radical of **4**(Lys•) in previous work.[33] Despite the small concentration of this intermediate, we have been able to use ENDOR to directly probe the arrangement of the components in state **4**(Lys•).

The **4**(Lys•) state contains a $[4Fe\text{-}4S]^{2+}$, cluster-bound methionine, adenosine, and the β-lysine α-carbon radical. The ENDOR experiments that interrogate this radical give an extremely large isotropic coupling to the 5′(^{13}C) of the 5′-Ado moiety, ~50% greater than observed in ENDOR spectra from the β-carbon radical of **3**(SLys•). The large couplings establish that this methyl is in van der Waals contact with both radicals; the difference in couplings indicates that the 5′-methyl is in better contact with the α-carbon radical of β-Lys• in **4**(Lys•) than with the β-carbon radical of α-Lys• in **3**(SLys•).

Results of the ENDOR studies of **4**(Lys•) prepared with $^{13}CH_3$-SAM are similar to those of **3**(SLys•) and **3**(DHLys•) in that they are compatible with the idea that the methionine formed by cleavage of SAM does not shift significantly on going from state **3** to state **4**.

Van der Waals Contact. The above findings disclose that hydrogen transfer is facilitated by the enforced van der Waals contacts of the reacting partners, and this has an important corollary. We suggest that the enforcement of van der Waals contacts *throughout* the hydrogen-transfer/isomerization mechanism enables the enzyme to minimize and even eliminate side reactions of highly reactive intermediates, such as the 5′-deoxyadenosyl radical. The radicals are limited to the allowed contacts by the substrate and coenzyme binding matrix in the active center of the enzyme and thereby prevented from undergoing reactions with other potentially reactive atoms. Radical mechanisms in enzymatic catalysis have long been considered problematic because of the perceived difficulty in controlling the reactivities of radicals. It seems that enzyme−substrate binding interactions remote from radical centers are sufficient to constrain the radical intermediates to productive reactions.

Van der Waals contact between a substrate radical and the methyl group of 5′-deoxyadenosine also is observed in the action of the adenosylcobalamin-dependent ethanolamine ammonia lyase.[27,34,35] The maintenance of close contacts to facilitate hydrogen transfer and "tame" reactive intermediates by preventing side reactions could be at work in the latter and likely in other radical reactions in enzymology.

Abbreviations Used. LAM, lysine 2,3-aminomutase; SAM, *S*-adenosyl-L-methionine; PLP, pyridoxal 5′-phosphate; Met, L-methionine; 5′-Ado, 5′-deoxyadenosine; Lys, L-α-lysine; β-Lys, L-β-lysine; ^{13}C-Met, L-*methyl*-^{13}C-methionine; ^{13}C-Ado, [5′-^{13}C]-5′-deoxyadenosine; ^{2}H-Ado, [5′,5′-2(^{2}H)]-5′-deoxyadenosine; DHLys, *trans*-4,5-dehydro-L-lysine; SLys, 4-thia-L-lysine; **3**(Lys•), α-lysine radical; **4**(Lys•), β-lysine radical; **3**(DHLys•), DHLys radical; **3**(SLys•), SLys radical; 5′-Ado•, 5′-deoxyadenosyl radical; anSAM, *S*-3′,4′-anhydroadenosylmethionine; anAdo•, 5′-deoxy-3′,4′-anhydroadenosine-5′-yl, EPR, electron paramagnetic resonance; ENDOR, electron nuclear double resonance.

Acknowledgment. This work has been supported by the NSF (MCB 0316038, B.M.H.) and NIH (HL 13531, B.M.H.; DK 28607, P.A.F.).

Supporting Information Available: Representative background spectrum for ^{13}C spectra of Figure 2 from an unlabeled sample (Figure S1) and discussion of the hyperfine parameters determined for the ^{13}C spectra (Figure 2) of **3**(SLys•), **4**(Lys•), and **3**(DHLys•), including a breakdown of the dipolar component into local and nonlocal contributions; discussion of the relationship between methyl ^{13}C and ^{1,2}H isotropic couplings for 5′-$^{13}CH_3$-Ado, and the one-deuteron model for fitting of the ^{2}H data. This material is available free of charge via the Internet at http://pubs.acs.org.

JA061282R

(33) Ballinger, M. D.; Frey, P. A.; Reed, G. H. *Biochemistry* **1992**, *31*, 10782−10789.
(34) LoBrutto, R.; Bandarian, V.; Magnusson, O. T.; Chen, X.; Schramm, V. L.; Reed, G. H. *Biochemistry* **2001**, *40*, 9−14.
(35) Warncke, K. *Biochemistry* **2005**, *44*, 3184−3193.